Design of a Hybrid Transducer Type Ultrasonic Motor

Kentaro Nakamura, Minoru Kurosawa, and Sadayuki Ueha

Abstract—**This paper presents a design method of a hybrid transducer-type ultrasonic motor (HTUSM) aimed at practical uses of the motor. We introduce a simple equivalent circuit that expresses the unique operation mechanism of the hybrid transducer-type motor. The numerical simulation based on the model enables us to predict the motor characteristics such as the maximum torque and the no-load revolution speed. In addition, for the purpose of efficient design and physical interpretation of the phenomena, we discuss analytically the maximum torque of a special case and develop two design charts for the prediction of the no-load speed of the motor.**

I. Introduction

IN AN ultrasonic motor, the revolution of a rotor is caused by a piezoelectric vibration of a stator instead of electromagnetic interaction. The driving force/torque is transmitted directly from the stator to the rotor by friction. This basic principle of the ultrasonic motor has unique properties, such as large output torque, large holding torque without energy consumption, and quick response. The major feature of an ultrasonic motor consists in the mechanism which converts stator vibration to rotor revolution. Only half a cycle of the vibratory motion of the stator should be transmitted to the rotor selectively. In traveling wave type ultrasonic motors [1]–[5], at every crest of the elastic traveling wave, the vibration velocity has the same direction which is opposite to that at the trough. Thus if we press a rotor on the stator that guides the traveling wave, it is driven to rotate. On the other hand, in a hybrid transducer-type ultrasonic motor [6]–[8] (HTUSM), the torsional vibration provides the driving force, while the longitudinal vibration changes the friction force between the rotor and the stator so that only half a cycle of the torsional vibration of the stator can be transmitted to the rotor. Ultrasonic motors using a longitudinal torsional vibration converter also belong to this type [9], [10].

These two typical conversion mechanisms are in contrast to each other. In the traveling wave type, driving forces having the same direction are extracted spatially from the stator vibration. In the HTUSM, on the other hand, it is done temporally. In other words, the temporal change of the friction between the rotor and the stator caused by the longitudinal vibration rectifies the torsional vibration into rotor rotation. Traveling wave type motors have been investigated widely, and some of them are in current use. The HTUSM, which was proposed by the authors about 5 years after the traveling wave type, has better characteristics such as high output torque and controllability. This paper presents a design method of the HTUSM by use of a simple model, to provide an aid for practical uses.

Focusing on the conversion mechanism from torsional vibration to rotor revolution, we employ an electrical equivalent circuit of the torsional vibrator, the rotor, and the friction characteristic of the contact surfaces. The friction force varies according to the normal force applied at the contact surface called the "preload." In this paper, for simplicity, it is assumed that the change in the preload due to the longitudinal vibration has a sinusoidal waveform. Analysis by this model shows that the conversion efficiency of the torsional port is above 80%, if the contact duration between the rotor and the stator is short enough. If the motor performance requirements such as maximum torque and no-load speed are given, the specifications of the torsional vibration system can be determined by using this model. For a systematic design procedure and a physical interpretation of the phenomena, we will consider analytically the maximum torque and develop design charts for the prediction of the no-load revolution speed.

II. Structure and Principle of the Motor

Fig. 1 illustrates a typical structure of a HTUSM. A stator has two types of piezoelectric elements to independently excite the torsional and the longitudinal vibration. A rotor is pressed to the transducer by a coil spring with a static force F_c. A normal force f_c at the contact surface between the rotor and the stator, termed "preload," varies periodically due to the longitudinal vibration, while a driving torque τ is generated by the torsional vibration. If the phase difference between displacements of the two waves is 90°, only half a cycle of the rotational force will be transmitted to the rotor from the stator in order to rotate the rotor in one direction. The rotation direction can be reversed, if we switch the phase difference by 180°.

III. Model of the Conversion Mechanism

To express the conversion mechanism from the torsional vibration to the rotor rotation, we introduce an equivalent circuit, shown in Fig. 2, which includes the torsional transducer, the rotor, and the friction characteristic at the contact surfaces. The torsional vibrator is driven by a high frequency voltage $V_T = V_0 \cos \omega t$. A "torque factor" A_r connects the

Manuscript received August 13, 1992; revised February 18, 1993; accepted March 24, 1993.

The authors are with the Precision and Intelligence Laboratory, Tokyo Institute of Technology, Midori-ku, Yokohama 227, Japan.

IEEE Log Number 9209828.

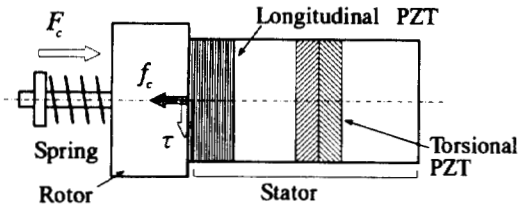

Fig. 1. Basic configuration of the motor.

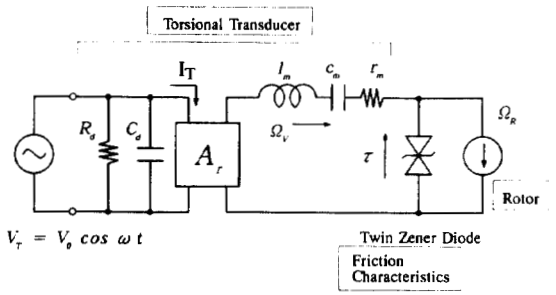

Fig. 2. Equivalent circuit of the motor for the torque generation mechanism.

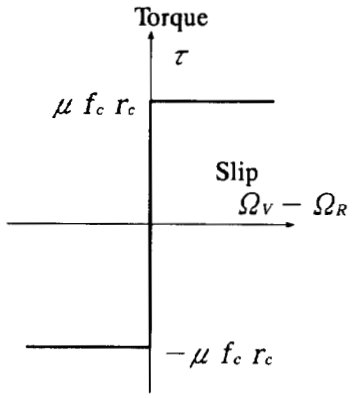

Fig. 3. Friction characteristic model of the contact surface used in the calculation.

electrical arm with the mechanical arm. The fundamental resonance mode of the torsional vibration system is represented by l_m, c_m, and r_m, while the clamped capacitance of the piezoelectric ceramics and its dielectric loss is denoted by C_d and R_d, respectively. The rotor is represented by a constant current source Ω_R under the assumption that the moment of inertia of the rotor is large enough in comparison with the driving frequency. In the figure, the angular vibration velocity is indicated by Ω_V. For the friction characteristics at the contact surface, we employ the Coulomb model as shown in Fig. 3, where traction force is limited to $\mu f_c r_c$ if slip exists. Here, μ, f_c, and r_c are the friction coefficient, the normal force at the contact surface (termed "preload"), and the contact radius, respectively. It is symbolized by a back-to-back-connected twin Zener diode in the circuit. To avoid the lengthy discussions on the analysis of the longitudinal vibration system [11], let us assume that the preload f_c varies temporally by the longitudinal vibration as shown in Fig. 4. Here, we define the contact duration ϕ_c during which the rotor is in contact with the stator. If the contact duration ϕ_c and the

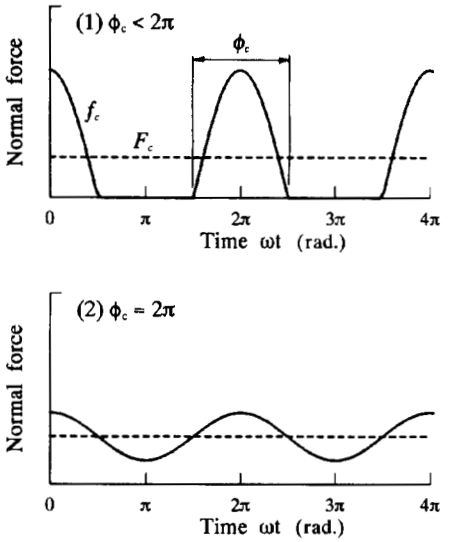

Fig. 4. Model of the preload waveform.

static load applied by the spring F_c are given, the time varying preload f_c can be uniquely determined as follows. First, as shown in Fig. 4, the waveform is assumed to be:

1) $0 < \phi_c < 2\pi$:

$$f_c = \begin{cases} \beta\left(\cos \omega t - \cos \frac{\phi_c}{2}\right), & \text{for } 0 < \omega t < \frac{\phi_c}{2} \\ & \text{or } 2\pi - \frac{\phi_c}{2} < \omega t < 2\pi \\ 0, & \text{elsewhere} \end{cases} \quad (1)$$

2) $\phi_c = 2\pi$:

$$f_c = F_c(1 + \kappa \cos \omega t). \quad (2)$$

It is obvious that the time averaged f_c is equal to F_c:

$$\overline{f_c} = F_c. \quad (3)$$

Here, the upper bar denotes taking the time average. Substituting (1) into (3), the amplitude β can be specified by ϕ_c and F_c. For $\phi_c = 2\pi, \kappa$ is proportional to the magnitude of the longitudinal vibration. To know the exact waveform of the preload, we should make a full analysis of the longitudinal vibration system including the effect of impact between the rotor and the stator. In this paper, however, we have employed a simple model, instead of a complex one, that is sufficient for the investigation of design method.

Then, an instantaneous torque τ is calculated from the circuit as follows. If slip exists, then

$$\tau = \begin{cases} \mu f_c r_c, & \text{slip} > 0 \\ -\mu f_c r_c, & \text{slip} < 0 \end{cases}. \quad (4)$$

In the case of no-slip (slip = 0), then

$$\tau = A_r V_0 \cos \omega t - l_m \frac{d\Omega_V}{dt} - \frac{1}{c_m} \int \Omega_V \, dt - r_m \Omega_V. \quad (5)$$

Here, slip is defined as the difference between the angular vibration velocity of the stator Ω_V and the angular velocity of the rotor Ω_R:

$$\text{slip} \triangleq (\Omega_V - \Omega_R). \quad (6)$$

Thus the output torque of the motor T can be calculated as the time average of the instantaneous torque τ:

$$T = \bar{\tau} \tag{7}$$

for the revolution speed of the rotor Ω_R.

IV. Fundamental Properties of the Motor

Before discussing the design method, let us mention the basic characteristics of the motor as determined by the model. First, Fig. 5(a) shows the plots of the speed load and the efficiency for $\phi_c = 180°$, simulated by using the model for various voltage V_T applied to the torsional port. The efficiency is the ratio of the output mechanical power to the input electrical power to the torsional port. No-load speed Ω_0 is defined as the revolution speed for $T = 0$, while the maximum torque T_0 is the load torque where the rotor revolution stops. The no-load speed and the maximum torque are proportional to V_T, though the saturation exists in the maximum torque because of the limit of the friction force. If V_T is too large, slip increases and the efficiency decreases. Fig. 5(b) shows in more detail the properties of the load curve in the case of high friction limit; $T_0 \ll \mu F_c r_c$. The revolution speed is reduced almost linearly as the load torque increases until it approaches the region near the torque axis. In the heavy load region near the maximum torque, the plot of the speed load is curved and the real maximum torque T_0 becomes greater than the effective maximum torque T_1 which is defined as the point where the extension of the linear part intercepts the torque axis as shown by a dashed line in the figure. In practice, it is convenient to regard the effective torque T_1 as the maximum torque, since the revolution speed is almost zero when the load torque is larger than T_1. The numerical value used in calculation here is summarized in Table I.

The calculated results fit well with the experimental ones. For example, as is shown in Fig. 6, the calculated speed load relation of a motor of 30 mm in diameter agrees well with the measured one for a prototype motor. The constants of the motor are listed in Table II.

Fig. 7 summarizes the effects of the contact duration ϕ_c on the motor performance, calculated with the parameters listed in Table I. The no-load speed N_0 becomes larger if the contact duration ϕ_c is shorter, and N_0 at $\phi_c = 0$ coincides with the angular vibration without load. The maximum torque T_0 has a peak at a certain ϕ_c. The contact duration ϕ_c has an optimum value of about $\pi/3$ rad for maximum efficiency. The maximum value of the efficiency is over 80%, and is close to the optimum efficiency of the torsional vibrator itself. This means that the hybrid transducer type has inherently high efficiency if the contact duration is short enough. However, in our prototype motors so far, the maximum efficiency was lower than 50% [12]. This means that the longitudinal vibration system did not succeed in reducing the contact duration. The overall efficiency of the motor was much smaller than this value, since electrical power was also dissipated in the longitudinal vibration system, which did not contribute to the motor output. Consequently, we should develop a strong longitudinal vibration system with high efficiency to improve the motor performance.

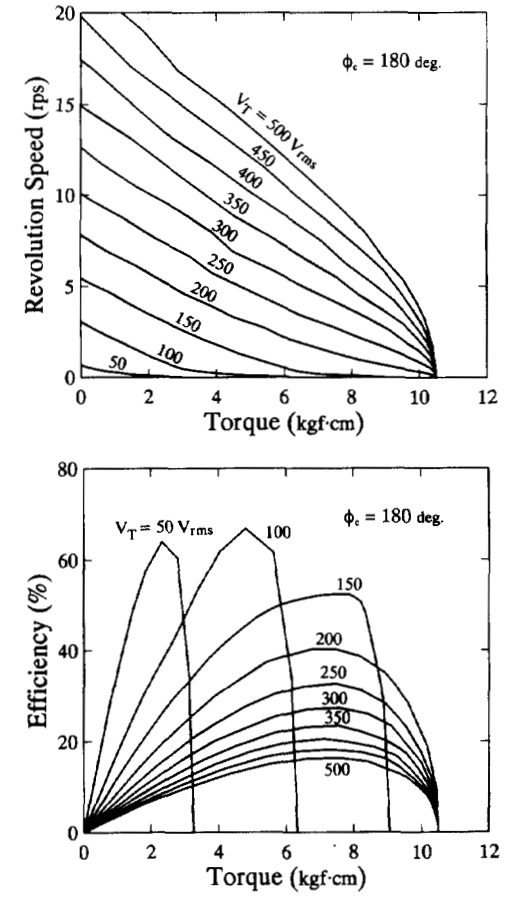

(a)

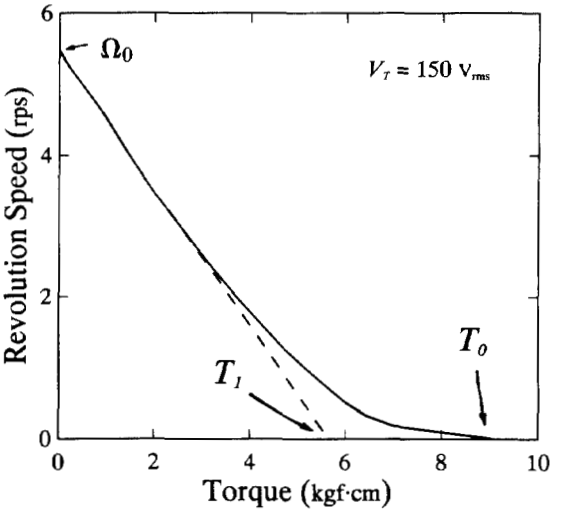

(b)

Fig. 5. (a) Calculated load characteristics and efficiency curves. (b) Details of a load characteristic curve, where T_0, T_1, and Ω_0 denote the maximum torque, the effective torque, and the no-load speed, respectively.

V. Design of the Motor Characteristics

A. Maximum Torque Design

We could determine the specifications of the torsional vibration system from the given maximum torque by means

TABLE I
PARAMETERS USED IN THE CALCULATION

Torque Factor A_r	0.0065 Nm/V
Free Admittance Y_{m0}	1.65 mS
Mechanical Q	50
Torsional Resonance f_{T0}	22.63 kHz
Clamped Capacitance C_d	3.3 nF
Dielectric Loss R_d	100 kΩ
Contact Radius r_c	14 mm
Friction Coefficient μ	0.15

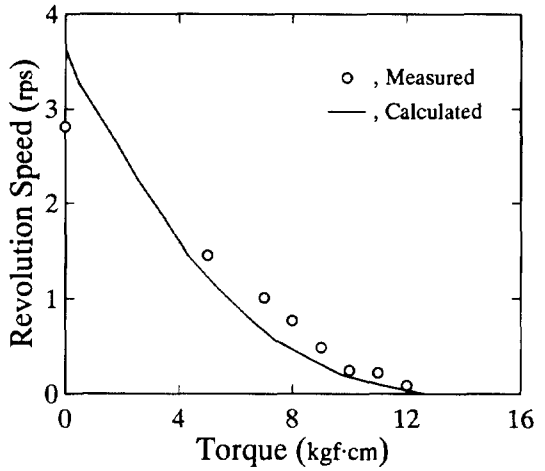

Fig. 6. Comparison between the calculated and measured results for a motor of 30 mm in diameter whose specification is described in Table II. $F_c = 40$ kgf, $\phi_c = 280°, V_T = 330\,V_{rms}$.

TABLE II
PARAMETERS USED IN FIG. 6

Torque Factor A_r	0.0048 Nm/V
Free Admittance Y_{m0}	0.60 mS
Mechanical Q	30
Torsional Resonance f_{T0}	20.60 kHz
Friction Coefficient μ	0.30

of the numerical calculation. However, it is useful to grasp the physical phenomena or meaning for an efficient design. If the reactive components in the equivalent circuit l_m and c_m are ignored, the maximum torque can be derived analytically for the special case $\phi_c \leqq \pi$. For small values of V_T, slip does not occur ($\Omega_V = \Omega_R = 0$: Maximum torque is a torque which stops the rotor), then:

$$\tau = \begin{cases} A_r V_T \cos \omega t & \text{(in contact)} \\ 0, & \text{(out of contact)} \end{cases}. \tag{8}$$

Consequently,

$$T_0 = \frac{A_r V_T}{\pi} \sin\left(\frac{\phi_c}{2}\right). \tag{9}$$

If V_T is so large that slip always exists:

$$\tau = \mu f_c r_c. \tag{10}$$

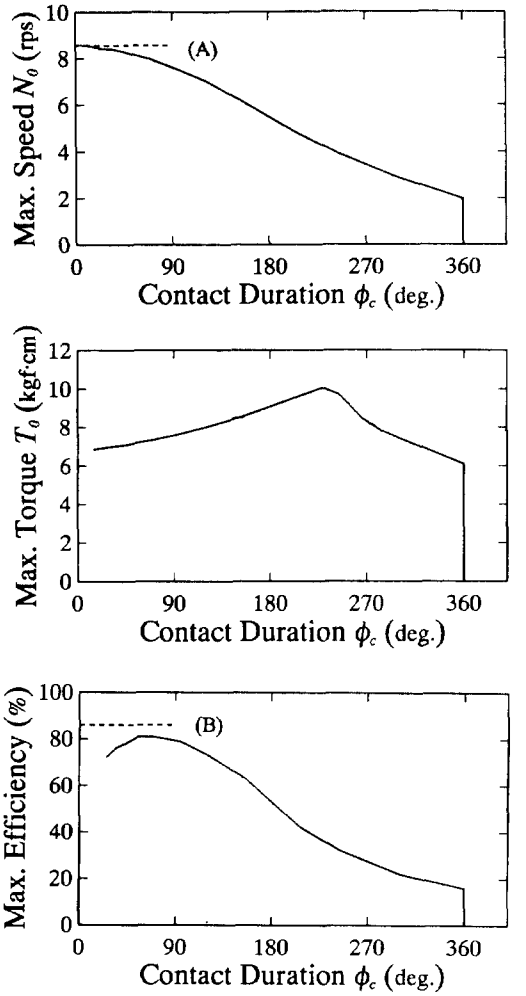

Fig. 7. Calculated motor performances as functions of the contact duration, where (A) and (B) express the free vibration velocity and the maximum efficiency of the torsional vibration system, respectively.

Then:

$$T_0 = \mu F_c r_c = T_{0\,\max}\,(\text{const.}). \tag{11}$$

These results show that maximum torque is proportional to the voltage and the torque factor, before it saturates at the friction limit. Fig. 8 shows the maximum torque (A), the effective torque (B) calculated with the reactive components c_m and l_m, and the maximum torque (C) without c_m and l_m. The left part ($\phi_c < \pi$) of the curve (C) is calculated by (9), while the expression of right part ($\phi_c > \pi$) of the curve (C) is not so simple that we need numerical integration. The effective torque T_1 decreases monotonically with ϕ_c, and T_1 can be approximated by the maximum torque calculated without the reactive components for the region of $\phi_c > \pi$. In a rough way, the value calculated by (9) for $\phi_c = \pi$ can be used for the practical design of the maximum torque. The procedure for the maximum torque design is summarized as follows: the preload by the spring F_c is determined first from (11), if the limiting torque $T_{0\,\max}$, is given. Then, (9) shows the required torque factor of the torsional vibration system A_r, if the torque factor as a motor T_0/V_T is given. The torque factor is determined by the size, the piezoelectric constant of the torsional PZT

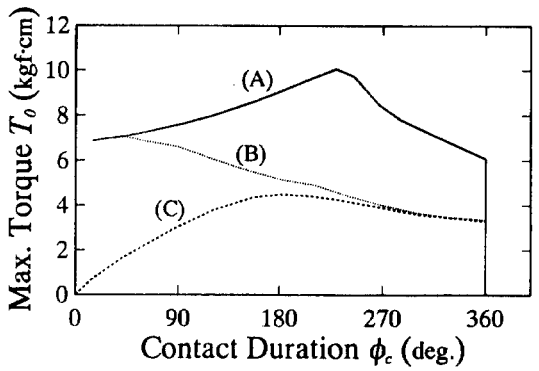

Fig. 8. Maximum torques versus the contact duration: (*A*) the maximum torque and (*B*) the effective torque calculated with the reactive components, (C) the maximum torque calculated without the reactive components.

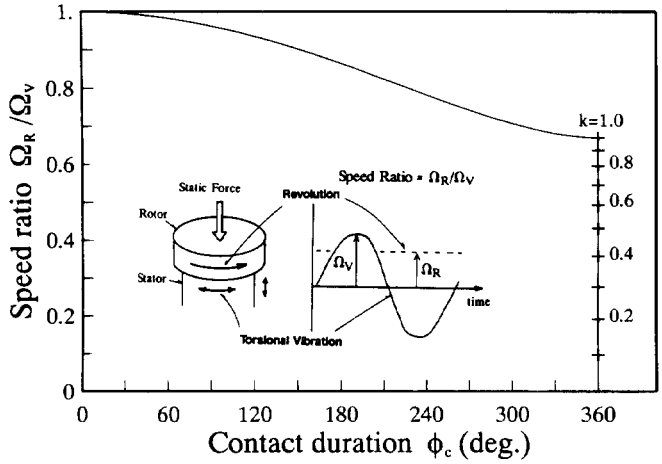

Fig. 10. Design chart (1): speed ratio as a function of the contact duration.

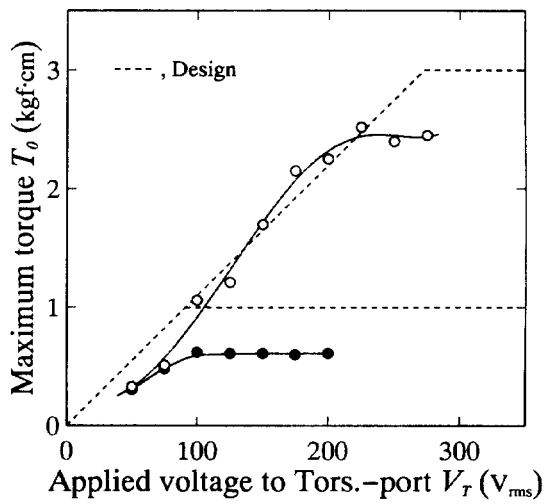

Fig. 9. Maximum torque as a function of the voltage applied to the torsional port. — o —, measured for F_c = 26.7 kgf; — • —, F_c = 8.9 kgf; dashed lines show design value.

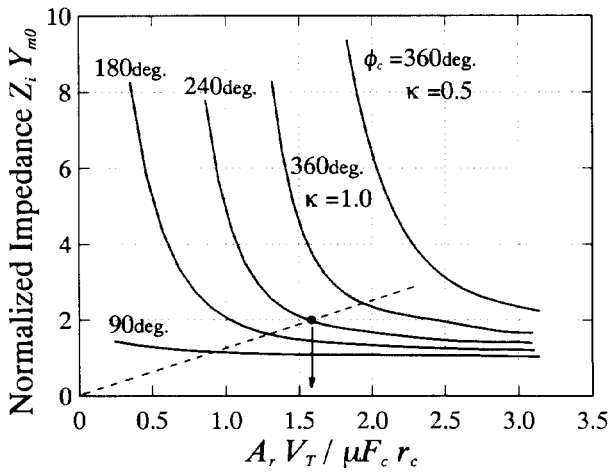

Fig. 11. Design chart (2): input impedance as a function of the applied voltage. A dashed line shows (14).

disk, and the vibration mode [12]. Fig. 9 compares the design maximum torque versus voltage with the actual data for a prototype motor. We could design the maximum torque successfully except at the saturation value. The limit of the maximum torque is lower than the design, since real contact duration is wider than the design value. Then, it is necessary to determine the preload F_c with a sufficient margin. This also means that we should operate the motor at the load torque sufficiently lower than $T_{0\,\max} = \mu F_c r_c$ in order to avoid slip and abrasion.

B. No-Load Speed Design

No-load speed can be defined as the revolution speed that makes the time average of τ zero. Hence, it is difficult to express the no-load speed in an analytic form in the same fashion of (9) and (11), and only a numerical solution is possible. However, to understand the mechanism, and to make the design procedure systematic, we divide the calculation into two steps and draw design charts. By using these charts, we can design a motor straightforwardly instead of repetition of numerical calculation.

First, let us introduce a new parameter "speed ratio" which is the ratio of the angular revolution speed of the rotor to the amplitude of the torsional vibration velocity of the stator. In Fig. 10, the speed ratio is plotted as a function of ϕ_c in the case of no-load, where the vibration velocity is assumed to be sinusoidal. If ϕ_c and the required no-load speed are given, we can find the necessary vibration velocity Ω_V from the plot. The motional current of the torsional port I_T is calculated by the relation:

$$I_T = A_r \Omega_V. \tag{12}$$

Second, we need to find the input impedance of the port to know the required voltage. Fig. 11 summarizes the calculated input impedance in a general form for the convenience of designers. For a universal usage, we use the impedance normalized by the free impedance of the torsional vibration system $1/Y_{m0}$ as the ordinate, and the ratio of the torque generated by the transducer $A_r V_T$ to the friction torque $\mu F_c r_c$ as the abscissa. The point where the limit $Z_i = V_T/I_T$ intersects a curve in Fig. 11 gives the required voltage V_T applied to the torsional port. Here, let us explain again how

to use the design charts (Figs. 10 and 11) with an example. For instance, parameters are given as $\phi_c = 240°$, $A_r = 0.007$ Nm/V, $Y_{m0} = 1.5$ mS, and $\mu F_c r_c = 0.96$ Nm. Then, no-load speed of 3 rps is required. First, the speed ratio Ω_R/Ω_V is found to be 0.78 by Fig. 10 ($\phi_c = 240°$). Consequently, we need the torsional vibration velocity Ω_V of 24.1 rad/s. By (12), the motional current of the torsional port I_T is calculated to be 0.169 A. Then, the input impedance Z_i is

$$Z_i = \frac{1}{0.169} V_T. \tag{13}$$

This can be rewritten into

$$Z_i Y_{m0} = 1.22\left(\frac{A_r V_T}{\mu F_c r_c}\right). \tag{14}$$

Next, we draw a line of (14) in Fig. 11. A point of intersection with the curve for $\phi_c = 240°$ gives the required voltage to be 220 V. Fig. 11 also exhibits the basic properties of the speed–voltage relation of the motor. The input impedance becomes large at a small voltage, especially for $\phi_c > \pi$. This implies that the rotor does not revolve in the low voltage region if $\phi > \pi$. Such a region becomes wider, if the contact duration ϕ_c is larger. If ϕ_c is small enough ($\approx \pi/2$), the input impedance changes little, and is almost equal to the free impedance of the torsional vibration system.

VI. Summary

We have introduced an electrical equivalent model of a hybrid transducer-type ultrasonic motor that expresses the mechanism of the torque generation by the torsional vibration. An analytic expression has been given for the torque design, while two design charts have been developed by numerical calculation for the no-load speed design. This paper revealed the basic characteristics of the motor and its physical interpretation. The maximum torque is limited by the friction properties at the contact interface. Until the limitation value, it is proportional to the voltage applied to the torsional port. The no-load speed is proportional to the current of the torsional port. The relation between the no-load speed and the voltage is not so simple, since the input impedance of the torsional port depends on the applied voltage. Based on the model, the design method of the motor has been presented, where the specifications of the torsional vibration system are determined by the motor performance.

A problem that is still to be solved in the future study is a precise analysis of the longitudinal vibration system. Up to this study, we cannot design the contact duration beforehand. In prototype motors, we could not make the contact duration shorter than π, and it was near 2π in most cases. A method needs to be established to systematically design the longitudinal vibration system.

References

[1] T. Sashida, Japanese patent 58-148682, Feb. 25, 1982.

[2] S. Iwamatsu, S. Ueha, M. Kuribayashi, and E. Mori, "Rotary ultrasonic motor using extensional vibration of a ring," *Jpn. J. Appl. Phys.*, vol. 25, suppl. 25-1, pp. 174–176, 1986.

[3] M. Kuribayashi, S. Ueha, and E. Mori, "Excitation conditions of flexural traveling waves for a reversible ultrasonic linear motor," *J. Acoust. Soc. Amer.*, vol. 77, no. 4, pp. 1431–1435, 1985.

[4] R. Inaba, A. Tokushima, O. Kawasaki, Y. Ise, and H. Yoneno, "Piezoelectric ultrasonic motor," *Proc. IEEE Ultrason. Symp.*, 1987, pp. 747–756.

[5] M. Kurosawa, K. Nakamura, T. Okamoto and S. Ueha, "An ultrasonic motor using bending vibrations of a short cylinder," *IEEE Trans. Ultrason. Ferroelec. Freq. Contr.*, vol. 36, pp. 517–521, 1989.

[6] M. Kurosawa and S. Ueha, "Hybrid transducer type ultrasonic motor," *IEEE Trans. Ultrason. Ferroelec. Freq. Contr.*, vol. 38, pp. 89–92, 1991.

[7] S. Takahashi, O. Ohnishi, O. Myohga, T. Uchikawa, T. Inoue, and I. Kagaya, "Ultrasonic motor using longitudinal-torsional composite vibration," in *Proc. Acoust. Soc. Jpn. Autumn Meeting*, vol. 2, Oct. 1988, pp. 821–822.

[8] Y. Tomikawa, K. Adachi, M. Aoyagi, T. Sagae and T. Takano, "Some constructions and characteristics of rod-type piezoelectric ultrasonic motors using longitudinal and torsional vibrations," *IEEE Trans. Ultrason. Ferroelec. Freq. Contr.*, vol. 39, pp. 600–608, 1992.

[9] A. Kumada, "A piezoelectric ultrasonic motor," *Jpn. J. Appl. Phys.*, vol. 24, suppl. 24-2, pp. 739–741, 1985.

[10] J. Tsujino and M. Takeuchi, "Ultrasonic rotary motor using a longitudinal-torsional vibration converter," *Jpn. J. Appl. Phys.*, vol. 31, suppl. 31-1, pp. 245–247, 1991.

[11] M. Kurosawa, K. Nakamura, and S. Ueha, "Numerical analysis of the property of a hybrid transducer-type ultrasonic motor," in *Proc. IEEE 1990 Ultrason. Symp.*, vol. 3, 1990, pp. 1187–1190.

[12] K. Nakamura, M. Kurosawa and S. Ueha, "Characteristics of a hybrid transducer-type ultrasonic motor," *IEEE Trans. Ultrason. Ferroelec. Freq. Contr.*, vol. 38, no. 5, pp. 188–193, 1991.

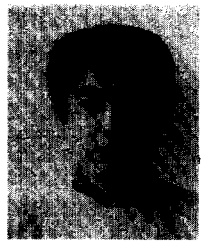

Kentaro Nakamura was born in Tokyo, Japan, on July 3, 1963. He received the B.Eng., the M.Eng., and the D.Eng. degrees from Tokyo Institute of Technology, Tokyo, Japan, in 1987, 1989 and 1992, respectively.

He has been a Research Associate of Precision and Intelligence Laboratory, Tokyo Institute of Technology, since 1992. His field of research is application of ultrasonics, and measurement of vibration and sound.

Dr. Nakamura is a member of The Acoustical Society of Japan, The Institute of Electrical Engineers of Japan, and The Institute of Electronics, Information, and Communication Engineers.

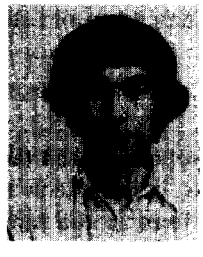

Minoru Kurosawa (formerly Kuribayashi) was born in Nagano, Japan, on April 24, 1959. He received the B.Eng. degree in electrical and electronic engineering, and the M.Eng. and D.Eng. degrees from Tokyo Institute of Technology, Tokyo, in 1982, 1984, and 1990, respectively.

He has been an Research Associate of the Precision and Intelligence Laboratory, Tokyo Institute of Technology, Yokohama, Japan, since 1984. His current research interests include ultrasonic motor, piezoactuator, high frequency and high intensity ultrasonic transducer, and other ultrasonic devices. Currently, he is an Associate Professor at the University of Tokyo in the Department of Precision Machinery Engineering, Tokyo, Japan.

Dr. Kurosawa is a member of the Institute of Electronics, Information, and Communication Engineers and The Acoustical Society of Japan. He has received the Awaya Kiyoshi Award for encouragement of research from The Acoustical Society of Japan in 1988.

Sadayuki Ueha was born in Kyoto Prefecture on February 28, 1943. He received the B.Eng. degree in electric engineering from Nagoya Institute of Technology in 1965 and the M.Eng. degree in 1967 and the D.Eng. degree in 1970, both in electric engineering, from Tokyo Institute of Technology.

He currently conducts research in high power ultrasonics, vibration measurement using physical optics, and acoustical imaging at the Tokyo Institute of Technology.

Dr. Ueha is a member of The Japan Society of Applied Physics, The Acoustical Society of Japan, The Institute of Electronics, Information, and Communication Engineers, and The Japan Society of Ultrasonics in Medicine. Currently, he is a member of the editorial board of *The Journal of The Acoustical Society of Japan*. He received The Best Paper Awards from The Japan Society of Applied Physics in 1975 and from The Acoustical Society of Japan in 1980, respectively.